Direct Numerical Simulation and Theoretical Analysis of Perturbations in Hypersonic Boundary Layers

Anatoli Tumin, Xiaowen Wang, and Xiaolin Zhong

Abstract Direct numerical simulations of receptivity in a boundary layer over a flat plate and a sharp wedge were carried out with two-dimensional perturbations introduced into the flow by periodic-in-time blowing-suction through a slot. The free stream Mach numbers are equal to 5.92 and 8 in the cases of adiabatic flat plate and sharp wedge, respectively. The perturbation flow field was decomposed into normal modes with the help of the multimode decomposition technique based on the spatial biorthogonal eigenfunction system. The decomposition allows filtering out the stable and unstable modes hidden behind perturbations having another physical nature.

1 Introduction

The progress being made in computational fluid dynamics provides an opportunity for reliable simulation of such complex phenomena as laminar-turbulent transition. The dynamics of flow transition depends on the instability of small perturbations excited by external sources. Computational results provide complete information about the flow field that would be impossible to measure in real experiments.

Recently, a method of normal mode decomposition was developed for two- and three-dimensional perturbations in compressible and incompressible boundary layers [6, 2, 7]. The method was applied to analysis of DNS data for perturbations introduced through the wall in the vicinity of the actuator [9]. The analysis demonstrated very good agreement between amplitudes of the modes filtered out from the

A. Tumin
The University of Arizona, Tucson, AZ 85721, USA, e-mail: tumin@email.arizona.edu

X. Wang
University of California, Los Angeles, CA 90095, USA, e-mail: xiaowen@seas.ucla.edu

X. Zhong
University of California, Los Angeles, CA 90095, USA, e-mail: xiaolin@seas.ucla.edu

DNS data and linear theory of the flow receptivity to blowing-suction through the wall.

In the present work, we apply the multimode decomposition to DNS results in a boundary layer past a flat plate and a sharp wedge downstream from the actuator in order to compare amplitudes of the modes found from the computations with the predictions of the linear stability theory.

2 Outline of the method

The method of multimode decomposition of perturbations having a prescribed frequency is based on the biorthogonal eigenfunction system for linearized Navier-Stokes equations [7]. For the clarity of further discussion, we reproduce the main definitions necessary for discussing the present work.

We consider a compressible two-dimensional boundary layer in the Cartesian coordinates, where x and z are the downstream and spanwise coordinates, respectively, and coordinate y corresponds to the distance from the wall. We write the governing equations (the linearized Navier-Stokes equations) for a periodic-in-time perturbation (the frequency is equal to zero in the case of a roughness-induced perturbation), $\sim \exp(-i\omega t)$, in matrix form as

$$\frac{\partial}{\partial y}\left(\mathbf{L}_0 \frac{\partial \mathbf{A}}{\partial y}\right) + \mathbf{L}_1 \frac{\partial \mathbf{A}}{\partial y} = \mathbf{H}_1 \mathbf{A} + \mathbf{H}_2 \frac{\partial \mathbf{A}}{\partial x} + \mathbf{H}_3 \frac{\partial \mathbf{A}}{\partial z} + \mathbf{H}_4 \mathbf{A} \tag{1}$$

where vector $\mathbf{A}$ is comprised of velocity components, pressure, temperature, and some of their derivatives; $\mathbf{L}_0, \mathbf{L}_1, \mathbf{H}_1, \mathbf{H}_2, \mathbf{H}_3$, and $\mathbf{H}_4$ are 16×16 matrices (their definitions are given in Ref. [8]). Matrix $\mathbf{H}_4$ originates from the nonparallel character of the flow. It includes terms with the y-component of the mean flow velocity and derivatives of the mean flow profiles with respect to the coordinate x.

In the quasi-parallel flow approximation, the solution of the linearized Navier-Stokes equations can be expanded into normal modes of the discrete and continuous spectra $\{\mathbf{A}_{\alpha\beta}, \mathbf{B}_{\alpha\beta}\}$ [7], where $\mathbf{A}_{\alpha\beta}$ and $\mathbf{B}_{\alpha\beta}$ are eigenfunctions of the direct and adjoint problems. Subscripts α and β indicate the eigenfunctions corresponding to the streamwise, α, and spanwise, β, wavenumbers, respectively. The eigenfunction system $\{\mathbf{A}_{\alpha\beta}, \mathbf{B}_{\alpha\beta}\}$ has an orthogonality relation given as

$$\langle \mathbf{H}_2 \mathbf{A}_{\alpha\beta}, \mathbf{B}_{\alpha'\beta} \rangle \equiv \int\limits_0^\infty \left(\mathbf{H}_2 \mathbf{A}_{\alpha\beta}, \mathbf{B}_{\alpha'\beta}\right) dy = \Gamma \Delta_{\alpha\alpha'} \tag{2}$$

where Γ is a normalization constant, $\Delta_{\alpha\alpha'}$ is a Kronecker delta if either α or α' belongs to the discrete spectrum, and $\Delta_{\alpha\alpha'}$ is a Dirac delta function if both α and α' belong to the continuous spectrum.

In a weakly nonparallel flow, one can employ the method of multiple scales by introducing fast (x) and slow $(X = \varepsilon x, \varepsilon \ll 1)$ scales. The mean flow profiles depend

on y and X only, whereas the perturbation will depend on both length scales. In the case of a discrete mode, solution of the linearized Navier-Stokes equation is presented in the form

$$\mathbf{A}_{\beta}(x,X,y) = \left[D_{v}(X)\mathbf{A}_{\alpha_{v}\beta}(X,y)\,e^{i\int \alpha_{v}(X)dx} + \varepsilon\mathbf{A}^{(1)}_{\alpha_{v}\beta}(X,y)\,e^{i\int \alpha_{v}(X)dx} + \ldots \right] \quad (3)$$

where the function $D_{v}(X)$ has to be determined. After substitution of Eq. (3) into Eq. (1), we arrive in order $O(\varepsilon)$ at an inhomogeneous equation for $\mathbf{A}^{(1)}_{\alpha_{v}\beta}$. The solvability condition of this equation allows finding $D_{v}(X)$ (one can find details and relevant references in [8]).

3 Numerical Approach

In the present work, we used the DNS results for flows past a flat plate and a sharp wedge with periodic-in-time perturbations introduced through the wall [10, 11]. The flow is assumed to be thermally and calorically perfect. The governing equations are the Navier-Stokes equations for a compressible gas in the conservative form. The fifth-order shock-fitting finite difference method of Zhong [12] is used to solve the governing equations in a domain bounded by the bow shock and the flat plate (or wedge). In other words, the bow shock is treated as a boundary of the computational domain. The Rankine-Hugoniot relations across the shock and a characteristic compatibility relation coming from downstream flow field are combined to solve the flow variables behind the shock. The shock-fitting method makes it possible for the Navier-Stokes equations to be spatially discretized by high-order finite difference methods. Specifically, a fifth-order upwind scheme is applied to discretize the inviscid flux derivatives. By using the shock-fitting method, the interaction between the bow shock and the wall forcing induced perturbations is solved as a part of solutions with the position and velocity of the shock front being solved as dependent flow variables. A second-order TVD scheme [13] is applied to simulate the steady base flow in a small region including the leading edge to supply inlet conditions for the shock-fitting simulation. The same numerical method was used in Refs. [3, 4, 5]. Both cases correspond to the adiabatic wall boundary condition.

4 Results

4.1 Flat plate

Free-stream flow conditions: Mach number $M_{\infty} = 5.92$, temperature $T_{\infty} = 48.69$ K, pressure $p_{\infty} = 742.76$ Pa. The Prandtl number and the specific heats ratio are 0.72 and 1.4, respectively. The periodic-in-time blowing-suction has been applied

through a slot having coordinates of the leading and trailing edges at 33 mm and 37 mm from the leading edge, respectively. The frequency of the perturbation was 100 kHz. Analyses of the mean flow velocity, temperature profiles and their derivatives have shown that they agree well with the self-similar solution for a boundary layer over a flat plate. Therefore, self-similar profiles have been used in the stability equations. In order to deal with the two-dimensional perturbations within the solver of Refs. [7, 8], the spanwise wave number β scaled with the Blasius length scale, $L = (\infty_\infty x / \rho_\infty U_\infty)^{1/2}$, was chosen equal to 10^{-5}.
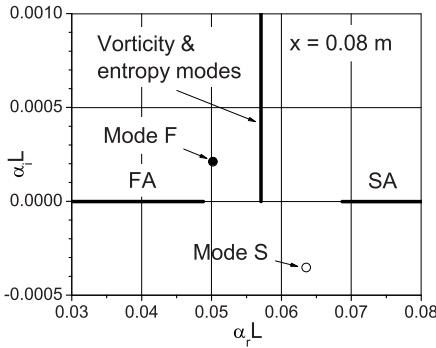
Fig. 1 Discrete modes and the continuous spectrum. FA and SA stand for fast and slow acoustic modes, respectively.
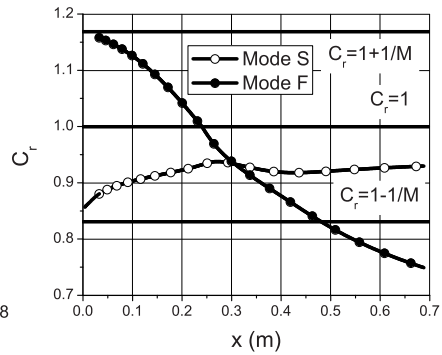
Fig. 2 Real parts of the phase velocities of the discrete modes F and S scaled with the free stream velocity U_∞.

In order to illustrate further analysis of DNS results, features of the spectrum should be introduced. Figure 1 shows the branches of the continuous spectrum and two discrete modes at $x = 0.08$ m. One of the discrete modes is labeled as mode F (fast), the other is labeled as mode S (slow). The modes' names stem from their phase velocity features in the vicinity of the leading edge. One can see in Fig. 2 that mode S is synchronized with the slow acoustic wave ($c_r = 1 - 1/M_\infty$), whereas mode F is synchronized with the fast acoustic wave ($c_r = 1 + 1/M_\infty$). At the chosen flow parameters, mode F is always stable, and mode S is the unstable mode. One can see that mode F is synchronized with vorticity/entropy modes having dimensionless phase velocity $c_r = 1$ at $x \approx 0.25$ m. The significance of the decaying mode F stems from its synchronization with mode S, where the decaying mode can give rise to the unstable mode (switching of the modes), which may lead to the transition [1].

Figure 3 shows pressure perturbation on the wall (scaled with the free stream pressure) obtained in the DNS (indicated as "measured") and projections on the discrete modes F and S. Amplification and decay of the discrete modes has been evaluated including the nonparallel flow effects as it is outlined in section 2. We do not show the amplitudes of the modes calculated within the quasi-parallel flow approximation. In the case considered, the nonparallel flow effect is significant. The "measured" data for the wall pressure perturbation have wiggles near the actuator
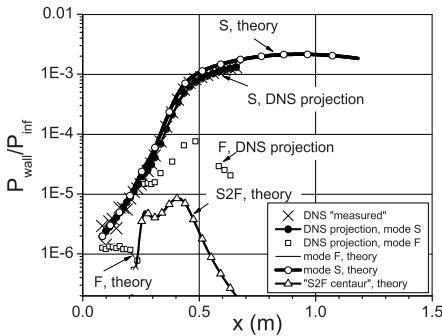
Fig. 3 Discrete modes and the continuous spectrum.
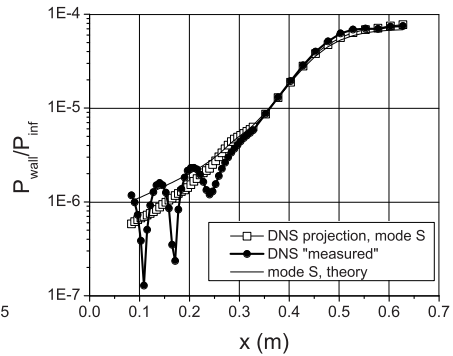
Fig. 4 Real parts of the phase velocities of the discrete modes F and S scaled with the free stream velocity U_∞.

region due to input from the various modes presented in the signal. The filtered out amplitude of the unstable mode S is smooth, and it is in good agreement with the theoretical prediction on the whole interval. It is interesting to look at the filtered out decaying mode F. It is in good agreement with the theoretical prediction (thin solid line) up to $x \approx 0.25$ m. After that, it has a jump and the amplitude becomes comparable with the amplitude of the mode S. The result can be attributed to the next term in the expansion (3). The second term, $\mathbf{A}_{\alpha_v\beta}^{(1)}(X,y)$, can be expanded into the eigenfunction system. It is a standard problem of finding eigenfunctions of a perturbed operator using the unperturbed basis. For the non-resonance case when eigenvalues of modes F and S are distinct ($\alpha_S \neq \alpha_F$), it is straightforward to find a projection of $\mathbf{A}_{\alpha_S\beta}^{(1)}(X,y)$ on $\mathbf{A}_{\alpha_F\beta}(X,y)$ (indices S and F indicate slow and fast discrete modes, respectively):

$$C_F(X) = \frac{D_S(X)}{i(\alpha_F - \alpha_S)} \frac{\left\langle \mathbf{H}_2 \frac{\partial \mathbf{A}_S^{(0)}}{\partial X}, \mathbf{B}_F^{(0)} \right\rangle + \left\langle \bar{\mathbf{H}}_4 \mathbf{A}_S^{(0)}, \mathbf{B}_F^{(0)} \right\rangle}{\left\langle \mathbf{H}_2 \mathbf{A}_F^{(0)}, \mathbf{B}_F^{(0)} \right\rangle} \tag{4}$$

where $\bar{\mathbf{H}}_4 = \varepsilon^{-1}\mathbf{H}_4$. For the purpose of brevity, we use only indices F and S indicating the fast and slow modes, respectively. The input of mode F into the second term of Eq. (3) has a wave number (and phase speed) corresponding to mode S. We call this contribution of the mode F as "S2F centaur" in order to emphasize the twofold character of the term. The wall pressure perturbation associated with "S2F centaur" is shown in Fig. 3 as well. Although the theoretical result for mode F downstream from the point of synchronism demonstrates qualitatively the same behavior as the amplitude of the DNS projection onto the mode F, there is a quantitative discrepancy that has yet to be understood.

4.2 Wedge

Free-stream flow conditions: Mach number $M_\infty = 8$, temperature $T_\infty = 54.8$ K, pressure $p_\infty = 389$ Pa. The Prandtl number and the specific heats ratio are 0.72 and 1.4, respectively. The periodic-in-time blowing-suction has been applied through a slot having coordinates of the leading and trailing edges at 51.84 mm and 63.84 mm from the leading edge, respectively. Frequency of the perturbation is 104.44 kHz.The wedge half-angle is equal to 5.3^o degrees. In this example, we use the velocity and temperature profiles obtained in the computation. The result of the DNS data projection onto the mode S and comparison with theoretical results is shown in Fig. 4.

The results of sections 4.1 and 4.2 illustrate how the multimode decomposition technique may serve as a tool for gaining insight into the flow dynamics in the presence of perturbations belonging to different modes.

References

1. A. Fedorov, A. Khokhlov, Theor. Comp. Fluid Dyn. **14**
2. P. Gaydos, A. Tumin, AIAA J. **42**
3. Y. Ma, X. Zhong, J. Fluid Mech. **488**, pp. 31-78
4. Y. Ma, X. Zhong, J. Fluid Mech. **532**, pp. 63-109
5. Y. Ma, X. Zhong, J. Fluid Mech. **488**
6. A. Tumin, Phys. Fluids **15**
7. A. Tumin, J. Fluid Mech. **586**
8. A. Tumin, J. Spacecraft and Rockets **45**
9. A. Tumin, X. Wang, X. Zhong, Phys. Fluids **19**
10. X. Wang, X. Zhong, AIAA Paper 2005-5025
11. X. Wang, X. Zhong, Phys. Fluids **21**
12. X. Zhong, J. Comput. Phys. **144**
13. X. Zhong, T. Lee, AIAA Paper 1996-1856